A Motion Monitor Using Hetero-Core Optical Fiber Sensors Sewed in Sportswear to Trace Trunk Motion

Yuya Koyama, Michiko Nishiyama, and Kazuhiro Watanabe

***Abstract*—In this paper, a cameraless motion monitor has been described by introducing very thin sensor modules into sportswear, in which a single-mode hetero-core optical fiber sensor is fabricated. An elbow joint motion and a trunk motion are monitored by a sportswear on which the hetero-core optical fiber sensor modules are sewed so as to be sensitive to stretch on the wear. In order to get rid of the restriction to the human body, a two-plane model has been proposed in which only two sets of sensors simplify three kinds of motions at the trunk, which are anteflexion, lateral bending, and rotation. Additionally, the real-time monitoring system has been tested when golf swing motion is performed. As a result, it has been indicated that the motion, which consists of a composite of three motions, can be significantly analyzed by means of the two sensors. The developed system is viable to an unconstrained motion capture system intended for a teaching device in sports and rehabilitation fields.**

***Index Terms*—Hetero-core fiber, motion monitor, optical fiber sensors, trunk motion, wearable.**

I. Introduction

ATTRACTIVE methods to capture human motion have been introduced in various aspects in daily life as a very useful tool in the fields of rehabilitation for the physically challenged people at home and of sports training, in which flexible mobility is favorably required so that people can easily use them in various places with no restriction imposed by the sensing mechanism to natural body movement. One of the motion capture methods is well known as 3-D data acquisition using multicamera systems to track the positions of the human body of interest with no physical contact with the body [1], which can reconstruct human body motion into digital data based on image analyses for many of the pictures. Although these camera systems are indispensable for taking an objective view of human motion, such systems are fraught with some difficulties in terms of cost and system complexity for daily use because they need to have many cameras to be installed around our life space. On the other hand, it could be useful for us to intuitively know our own motion in supporting sports training and rehabilitation, the system for which should be called "motion monitor."

In contrast to the camera system, cameraless methods typically utilize inertial sensors such as an accelerator and gyro-sensors mounted on two-wheeled vehicles for roll-angle detection [2] or on body segments [3]–[8] for detecting the angles of body joints. Additionally, some approaches have been also proposed as wearable sensing systems using wireless inertial modules [3], [6], [8]. Despite the fact that inertial sensors need compensation for accumulated errors because of their need for integration computation in principle, they have been already commercialized in the market with growing demands for cameraless motion capture systems. However, they have difficulties in getting rid of constraint to motion because of their bulky sensor structures at the joint portions. Optical reflection sensing systems using the light source and the detector placed on a measurement object or external environment have been also proposed as cameraless methods for tracing painted trajectory [9], [10], object's angles [11], and the strain of periodic objects [12]. However, these systems need to be used in such limited environments that have constant optical reflectivity and the light source installed around the object.

Alternative cameraless ways [13]–[15] were previously reported in the forms of wearable sensing garments based on electrically conductive sensors, which detected the stretch of the garment due to body movements from the change in electrical resistance caused by the strain given to the sensor. Aside from the need for a compensation procedure for the elastic limit of thin metal or conductive polymer materials, they can be an elaborate system closest to the word "wearable," which the present technique, so far, can offer in order to realize a sensor wear.

In addition to these conventional ways of the mounted sensors or the sensor wear mentioned above, optical fiber sensors were examined to develop wearable sensing systems because the fiber nature of thin size and lightweight was suitable to be sewed on cloth with no constraint. Fiber Bragg gratings (FBGs) [16] and cut-in plastic optical fiber (POF) [17] were previously used for that purpose. It is well known that human body movement can be too large to be detected by FBG sensors since the displacement sometimes exceeds the range of a few millimeters or centimeters, which can be out of the coverage with FBG. The need for temperature compensation could be an additional complexity for system integration. The POF sensor system can be used in the form of tape, which was attached on the body to detect joint angles. Fluctuation due to the loss change of transmission line except for the cut-in sensor portion is unavoidable since POF is based on the multimode

Manuscript received December 8, 2011; revised February 29, 2012; accepted March 14, 2012. Date of publication February 21, 2013; date of current version March 8, 2013. The Associate Editor coordinating the review process for this paper was Dr. S. Shirmohammadi.

Y. Koyama and K. Watanabe are with the Department of Information Systems Science, Faculty of Engineering, SOKA University, Tokyo 192-8577, Japan.

M. Nishiyama is with the Aerospace Research and Development Directorate, Japan Aerospace Exploration Agency, Tokyo 181-0015, Japan.

Color versions of one or more of the figures in this paper are available online at http://ieeexplore.ieee.org.

Digital Object Identifier 10.1109/TIM.2013.2241534

operation. An optical fiber goniometer due to the change in polarized status using fiber loops based on single-mode (SM) fiber operation [18] was developed for detecting human motion. However, this technique has difficulty in detecting complex human exercises such as trunk motion because the goniometer can only detect human joint movement.

Hetero-core optical fibers [19], [20] have been developed with the ability of detection in the range of a few millimeters or more, which make it possible to capture body motion. In addition, the hetero-core optical fiber has advantages of high sensitivity to soft bending on sensor portion, no necessity for temperature compensation, and stable SM fiber operation along the transmission line [21]. This technique can be attractively applied to motion capture or monitor system in the form of a wear without constraint when such a thin and lightweight sensor element is placed at a small number of body locations of importance.

In this paper, a sportswear has been described, which is viable to an unconstrained motion capture system by sewing hetero-core optical fiber sensor modules on the wear. The developed system can monitor the trunk movement of the human body, which is the most important part to determine the posture of humans. A sensor element is placed in a thin plastic case, which can be sewed or hocked to be sensitive to cloth stretch. The thin module was first tested to ensure wear stretching due to elbow flexion motion. In order to reduce the number of sensor modules sewed, hence remove constraint as much as possible, a method has been introduced in which the trunk of the body is approximated to two planes. Such two planes work to simplify three kinds of motions at the trunk, which are anteflexion, lateral bending, and rotation, using only two sets of sensing portion. As a result, it has been shown that the two-plane model with two sensor portions could independently discriminate three freedom of movements. Additionally, the developed system has been also applied to monitor the trunk motion when golf swing is performed. It has been implied that the developed system would be expected to apply not only to motion monitor but also to an alternative way of motion capture system for a teaching device to correct own behavior into an instructed motion.

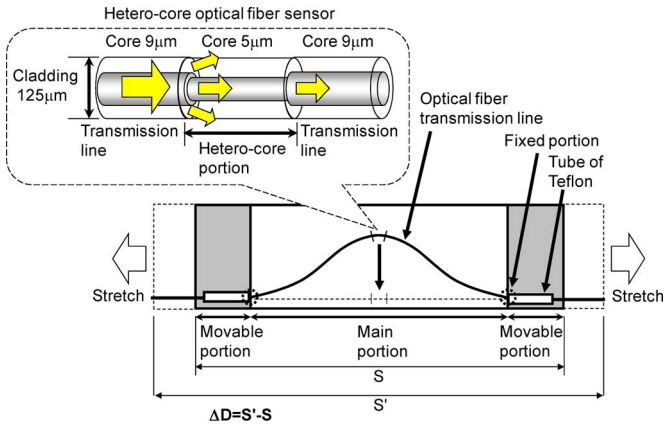

Fig. 1. Structures of hetero-core optical fiber and the stretching module.

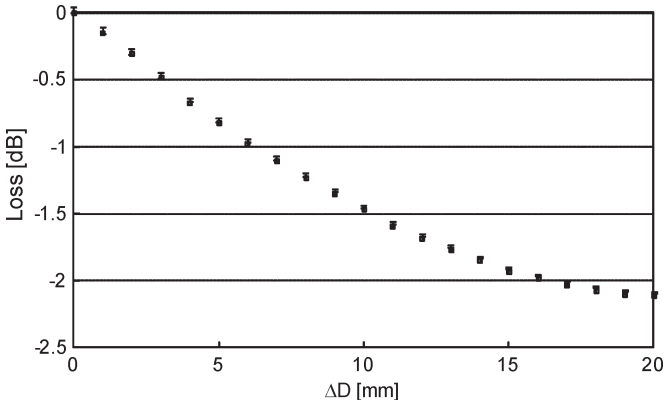

Fig. 2. Optical loss performance against the displacement of the hetero-core fiber optic stretching module with 20 trials.

II. Stretching Module Using Hetero-Core Optical Fiber Element

A. Module Structure

As shown in the upper inset in Fig. 1, a 2-mm short segment of fiber with a core diameter of 5 μm is inserted in a 9-μm-core SM fiber transmission line by means of fusion splicing, which is named hetero-core portion. The hetero-core portion at which leakage easily occurs by giving soft bending since transmission light can partially leak into a cladding at a boundary interface fusion-spliced portion. In our previous work, it was shown that the curvature change was converted into optical loss change, which increased almost linearly to bending action due to displacement with no temperature compensation [20].

The configuration of a stretching module is indicated in Fig. 1 for detecting expansion and contraction. A hetero-core element is housed in a plastic case whose dimension is $60^{\mathrm{w}} \times 100^{\mathrm{l}} \times 4^{\mathrm{t}}$ mm, which wholly weighs 18 g. The movable portions on both sides can be stretched and spring backed so that soft bending at the center can be altered according to the stretch given in the coverage of 20 mm. The initial position was set at the shortest position with no stretch. The initial and extended lengths of the module are denoted by S (100 mm) and S', respectively, giving the displacement $\Delta D = S' - S$.

B. Performance Characteristics of a Stretching Module

Fig. 2 shows the optical loss as a function of the stretch displacement ΔD, in which the loss is decreased with increasing ΔD. The stretch was linearly given to the module by a mechanical stage from the initial distance of 40 mm up to 60 mm with a stepwise resolution of 1 mm. The plots in Fig. 2 are given as the averaged value over 20 times. The optical loss was obtained using a light-emitting diode (LED) at the wavelength of 1.31 μm, which was coupled into a transmission fiber and an optical power meter (OP710, Opto Test Co.). It is confirmed from Fig. 2 that a standard deviation of 0.55% is obtained, which corresponds to 0.11 mm for the full scale of 2.1 dB for $\Delta D = 20$ mm. This result shows that the accuracy of the stretching module is sufficient to capture motions at a body joint or at trunk.

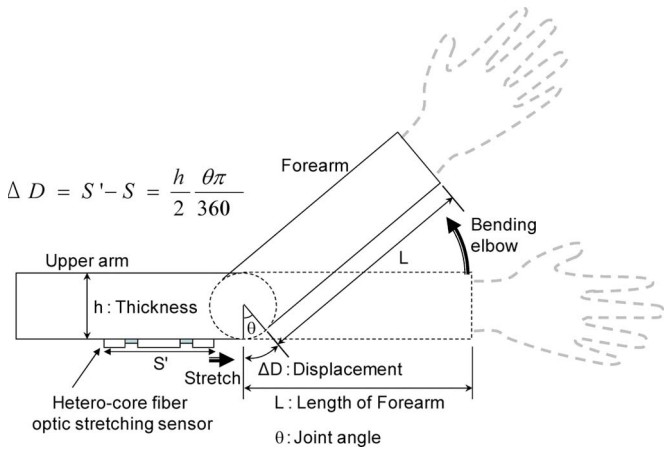

Fig. 3. Geometrical drawing to show the relation ΔD and θ for elbow flexion.

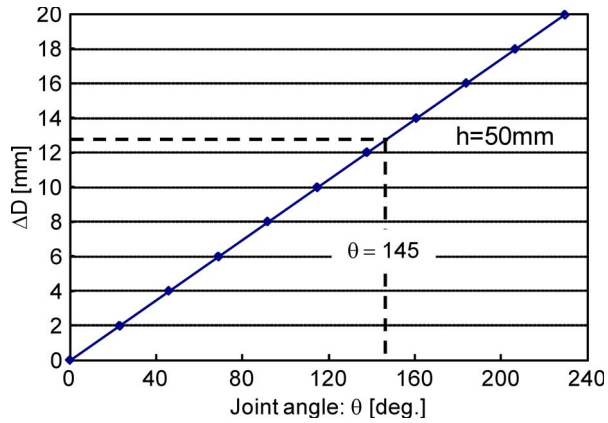

Fig. 4. Optical loss as a function of the joint angle θ calculated from $\Delta D = (h/2) \cdot (\theta\pi/360)$.

III. Stretching Test of a Sportswear to Capture the Flexion of Elbow

Fig. 3 shows a schematic drawing for converting the angle of the elbow flexion to ΔD. The thin sensor module was sewed under the upper arm portion of a sportswear so that the wear could be stretched when the elbow flexion is given. As shown in Fig. 3, ΔD is approximated to the circular arc, which is given as

$$\Delta D = \left(\frac{h}{2}\right) \cdot \left(\frac{\theta\pi}{360}\right) \tag{1}$$

where h and θ are the thickness of the arm and the angle of the bending elbow, respectively. The simple relation between θ and ΔD given by (1) is plotted in Fig. 4 to ensure that the full range of elbow motion (typically $\theta = 145°$) for healthy people could be covered with the maximum stretching $\Delta D = 20$ mm. The accuracy of the elbow flexion angle could be estimated to be 1.26°, which corresponds to the standard deviation of 0.55%, as mentioned above.

Fig. 5 shows an experimental setup with which a sportswear stretching test of elbow flexing motion was made using the sensor module sewed in a sportswear (SkinsTM, XXS size, CUSTOM PRODUCE Co.) by fasteners.

The motion in this experiment was given as (i) extending the elbow straight and (ii) fully bending the elbow. The real-time response of elbow motion is indicated in Fig. 6, in which the repeated motion of elbow (i) extension and (ii) flexion is detected in the range 0°–149°. This successful motion capture implies that the sportswear sewed this technique is sensible to the stretch of cloths so that other joints such as the knee or the leg could be captured in the same way as the elbow motion.

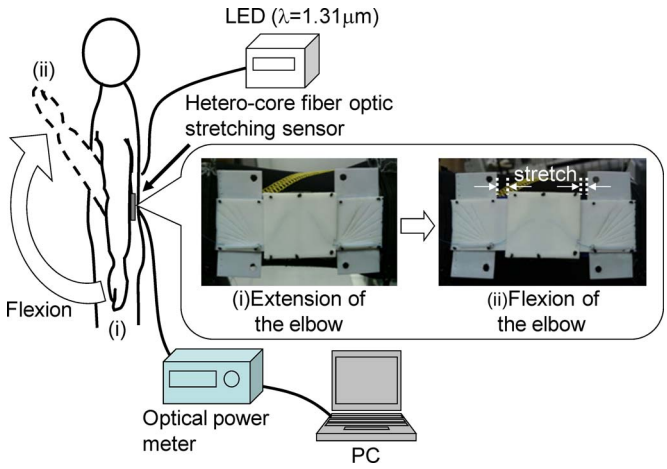

Fig. 5. Experimental setup for the experiment for real-time elbow response detected by stretching module.

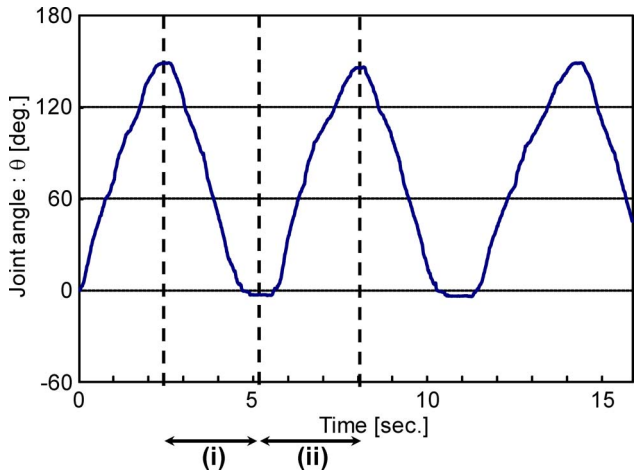

Fig. 6. Real-time response of joint angle for the repeated motion of elbow flexing.

IV. Experiments to Capture the Trunk Motion

A. Two-Plane Model to Approximate the Trunk of Body

A simple method is introduced to assume the complex movement of trunk by using two imaginary planes as if they were placed at the back of the body, as shown in Fig. 7. This model is needed to analogically infer the trunk motion by specifying two distances on the planes as P_1Q_1 and P_2Q_2, which could vary with stretch due to motion. The lengths of P_1Q_1 and P_2Q_2 can be detected by the two sensor modules and extension nylon strings that connects P_1, P_2 and Q_1, Q_2. This model makes it possible to analyze complex trunk motion with only a pair of sensor modules, hence successfully to get rid of constraint to human motion as much as possible. These imaginary planes are found to be useful in converting displacements of P_1Q_1

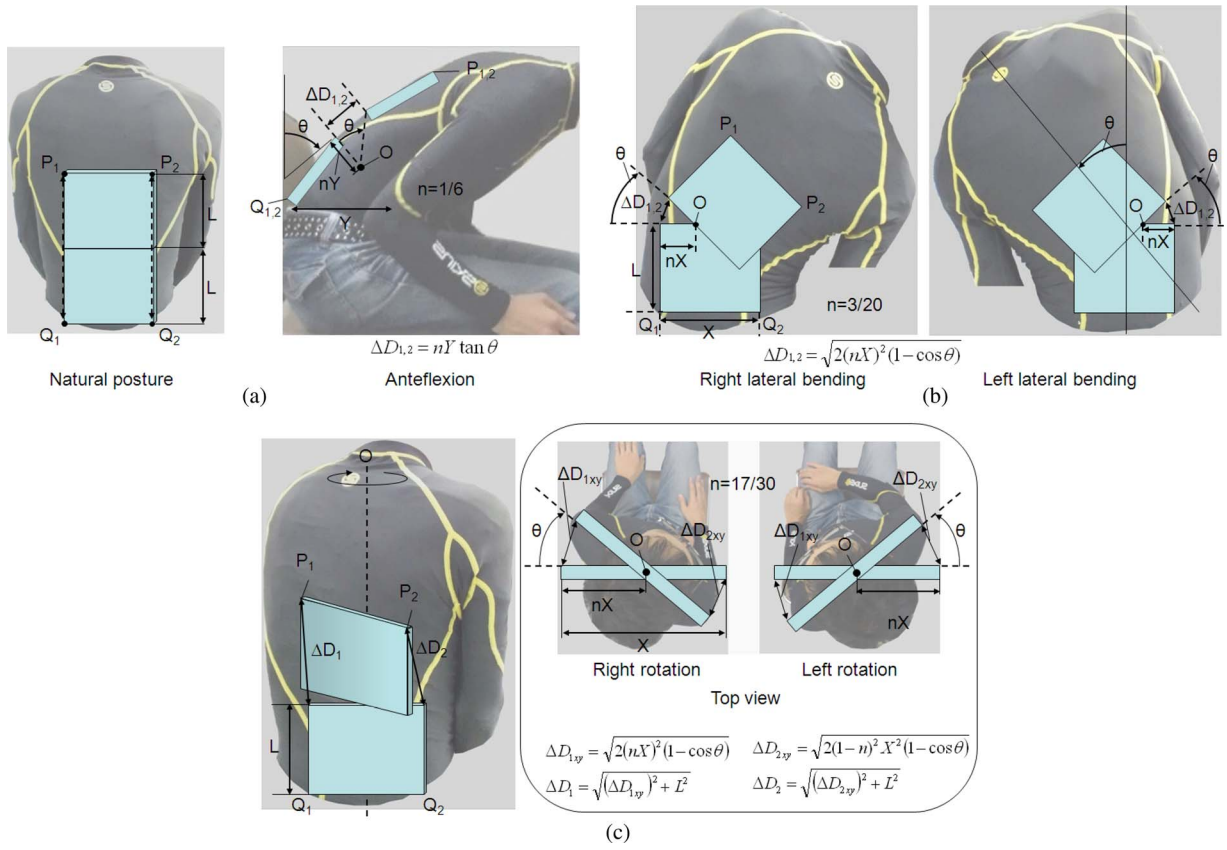

Fig. 7. Simple model in which two imaginary planes convert displacements of P_1Q_1 and P_2Q_2 into angles for the (a) anteflexion, (b) lateral bending, and (c) rotation of the trunk motions.

and P_2Q_2 into angles for the anteflextion, lateral bending, and rotation of the trunk motion. Comparing P_1Q_1 with P_2Q_2, the three motions can be simply distinguished, which are conceivable fundamentals for the trunk action in this work. Fig. 7 shows the movements of two planes at the back, which correspond to (a) anteflexion, (b) lateral bending, and (c) rotation. As shown in Fig. 7(a), the initial lengths of P_1Q_1 and P_2Q_2 are given as $2L$ in natural posture. The sensor modules are initially set to zero (no displacement) when the lengths are $2L$.

The position of the upper plane changes when each motion takes place, whereas the lower plane remains at the initial position, so that the increased lengths ΔD_1 and ΔD_2 for P_1Q_1 and P_2Q_2 are correlated with motion angle θ by using a simple geometric calculation. As shown in Fig. 7(a), the surface of the back stretches along the direction of anteflexion, so that the location of the upper plane moves upward with motion angle θ, which is defined as the tangential angle to the vertical direction of body. The axis O is tentatively placed at the distance of nY from the back. ΔD_1 and ΔD_2 are simply given as

$$\Delta D_{1,2} = nY \tan\theta \tag{2}$$

where Y and n are the body depth of 110 mm and a fitting parameter, respectively. The fitting parameter is chosen so as to adapt a realistic $\Delta D_{1,2} - \theta$ relation obtained by experiments. Fig. 7(b) shows the lateral bending motion in which the location of the upper plane rotates with θ around the axis O. In the same way as the anteflexion, the location of the axis O is given by distance nX using fitting parameter n. In lateral bending, the line for the stretched side is increased, whereas the line on the other side remains with no stretch, which means that $\Delta D = 0$. The increased lengths ΔD_1 and ΔD_2 are approximately given as

$$\Delta D_{1,2} = \sqrt{2(nX)^2(1-\cos\theta)} \tag{3}$$

where X and n are given as the plane width of 157 mm in this case and a fitting parameter. As shown in Fig. 7(c), the upper plane rotates along the direction of rotation because the surface of the back is twisted back and forth. The right inset in Fig. 7(c) shows the top view above the planes in which the upper plane rotates around the axis O placed at the position of nX from the right and left side. Thus, ΔD_1 in the right rotation is expressed as

$$\Delta D_1 = \sqrt{(\Delta D_{1xy})^2 + L^2}$$

where

$$\Delta D_{1xy} = \sqrt{2(nX)^2(1-\cos\theta)}. \tag{4}$$

Similarly, ΔD_2 is given as

$$\Delta D_2 = \sqrt{(\Delta D_{2xy})^2 + L^2}$$

where

$$\Delta D_{2xy} = \sqrt{2(1-n)^2X^2(1-\cos\theta)}. \tag{5}$$

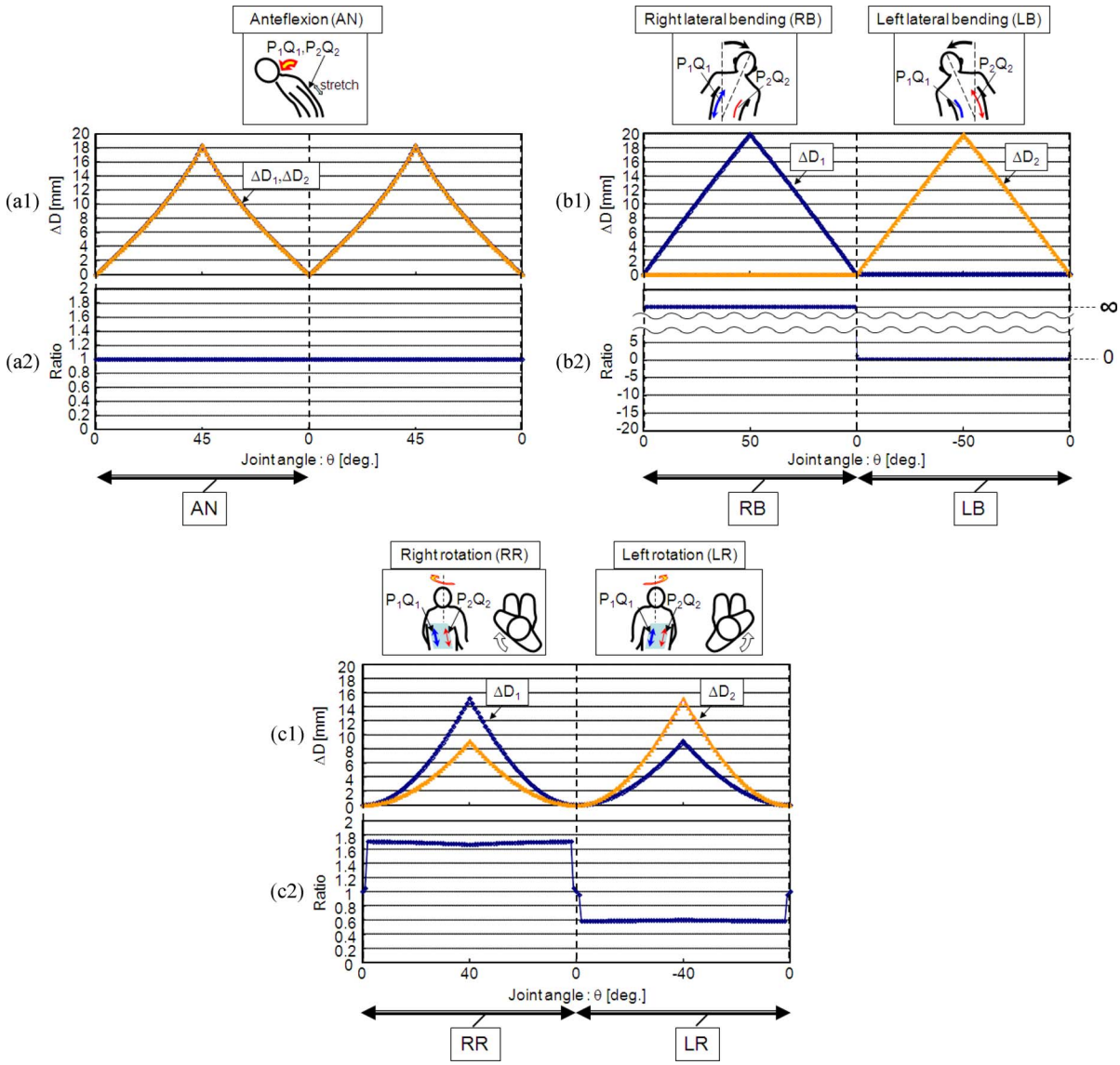

Fig. 8. Calculation results for the trunk motion, showing $\Delta D_{1,2}$ and ratio $\Delta D_1/\Delta D_2$. (a1) and (a2) For anteflexion. (b1) and (b2) For lateral bending. (c1) and (c2) For rotation.

Fig. 8(a1), (b1) and (c1) shows the results of the model calculations for ΔD_1 and ΔD_2 as a function of motion angle θ in the range of experiment: $0^\circ \leq \theta \leq 45^\circ$ for the anteflexion, $-50^\circ \leq \theta \leq 50^\circ$ for the lateral bending, and $-40^\circ \leq \theta \leq 40^\circ$ for the rotation. The changes in ΔD_1 and ΔD_2 from the model indicate that the increase in two distances $\mathrm{P_1Q_1}$ and $\mathrm{P_2Q_2}$ characterizes three types of motion. The ratio $\Delta D_1/\Delta D_2$, as shown in Fig. 8(a2), (b2), and (c2), could be convenient to clearly distinguish the states of motion. The ratio, for instance, shows 1 for anteflexion, infinity for right lateral bending, 0 for left lateral bending, $\cong$1.7 for right rotation, and $\cong$0.6 for left rotation, the regions of which are indicated by AN, RB, LB, RR, and LR, respectively.

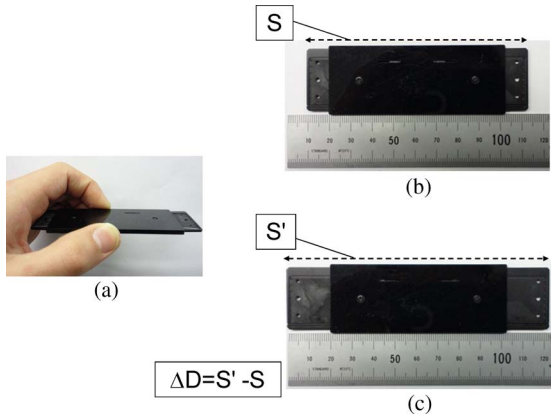

Fig. 9. Thin stretching sensor module for trunk motion experiment. (a) Side view. (b) Top view. (c) Extended state.

B. Experimental Setup for the Trunk Motion

Fig. 9 explains the sensor module in which the side view, the top view, and the extended state are shown in (a), (b), and (c), respectively. Fig. 10(a) shows the overview of the experimental setup for capturing the trunk motions by using the above modules. A multichannel LED/PD measurement system at the wavelength of 1.31 μm was employed for the sake of

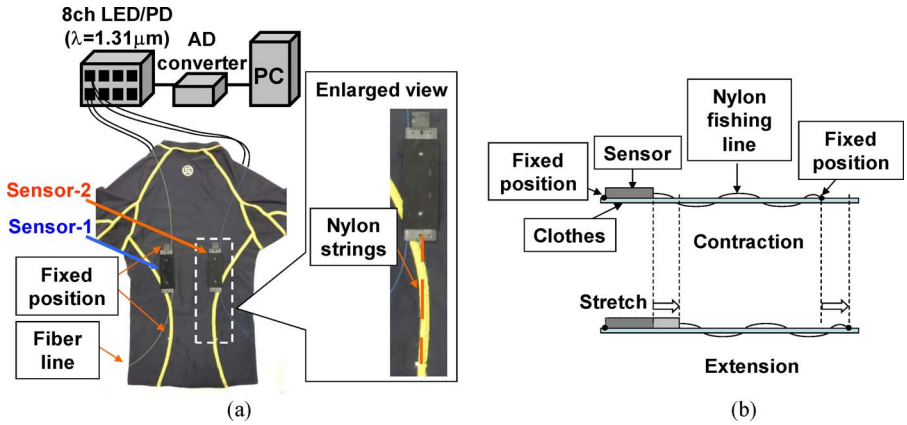

Fig. 10. Experimental setup for trunk motion measurement by using two stretching sensors. (a) Overview and (b) the cross-section view of sensor module on wear.

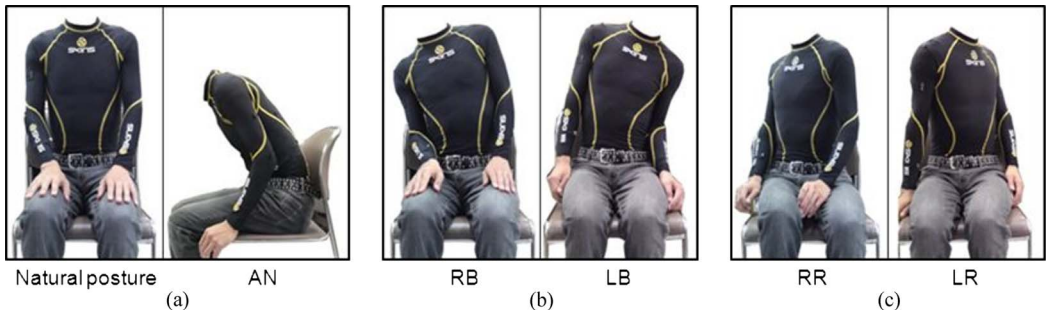

Fig. 11. Three types of trunk motion in the real-time experiment. (a) Anteflexion. (b) Lateral bending. (c) Rotation.

simultaneous measurement in real time for the two modules. The modules indicative of sensor-1 and sensor-2 are arranged below the shoulder blade portion of a sportswear in parallel symmetry to the spine at the center. A nylon string attached with one movable portion was sewed into the clothes, and the other end is fixed at the position of the waist in order for the module to detect the change in the distance covering the whole range of the back. Fig. 10(b) shows the cross-sectional view in which the sensor module is set on the clothes so that the change in length between two fixed positions can be detected by the stretch. The motion of three kinds at the trunk was performed from the natural posture that the human on the chair keeps by extending the spine naturally, as shown in Fig. 11. Each motion was given as bending and extending the thoracolumbar region back and forth (AN) for anteflexion, bending the thoracolumbar region right (RB) and left (LB) for lateral bending, and turning the thoracolumbar region right (RR) and left (LR) around the spine for rotation.

V. Results and Discussion

Fig. 12(a1), (b1), and (c1) shows ΔD_1 and ΔD_2 corresponding to the trunk motion obtained in a real-time base with a sampling frequency of 30 Hz. The change in ΔD_1 and ΔD_2 could be characterized as three kinds of motion in the same way as the results of the calculation mentioned above. Fig. 12(a2), (b2), and (c2) shows the experimental results of the ratio $\Delta D_1/\Delta D_2$ with removing the high-frequency component produced at the vicinity of ΔD_1, $\Delta D_2 \cong 0$ using a 6-Hz low-pass filter. A threshold value of 40 is set for (b2) to limit the large value of $\Delta D_1/\Delta D_2$, which theoretically corresponds to infinity. $\Delta D_1/\Delta D_2$ is obtained only in the region between the dashed lines where the one sensor produces large signals more than 2 mm enough to remove the fluctuation near zero for each sensor characteristics. The ratios are shown as the range of $0.64 < \Delta D_1/\Delta D_2 < 1.24$ for anteflexion, $8.2 < \Delta D_1/\Delta D_2 < 40$ for right lateral bending, < 0.09 for left lateral bending, $2.4 < \Delta D_1/\Delta D_2 < 25$ for right rotation, and $0.1 < \Delta D_1/\Delta D_2 < 0.57$ for left rotation, the areas of which are indicated by AN, RB, LB, RR, and LR, respectively. It is found in Fig. 12 that the three types of motions are indicated by the values $(\Delta D_1/\Delta D_2)$ that are similar to the two-plane calculations explained in Fig. 8. With evaluating these values, how trunk motion could be dominated by the three fundamental motions.

Fig. 13 shows the relation of AN, RB, LB, RR, and LR obtained by (a) the calculations of the two-plane model and (b) the experiments. Although the $\Delta D_1/\Delta D_2$ for the experiments are dispersed in some ranges, which are separately ranged for three types of motion, the range appeared in the experiments could be caused by such a factor as inevitable imbalance due to sensor placement on a soft material of the sportswear. These results indicated that two sewed stretch sensors arranged in parallel on the back could grasp which kind of motion dominates the motions of the trunk by evaluating the ratio.

VI. Golf Swing Monitoring Experiment

Real-time monitoring of golf swing has been demonstrated by using the sensor wear. System configuration and the position of the sensors are the same as the above. The golf swing motion consists of the following process: (i) taking a back swing, (ii) leading up to an impact, and (iii) following through, as

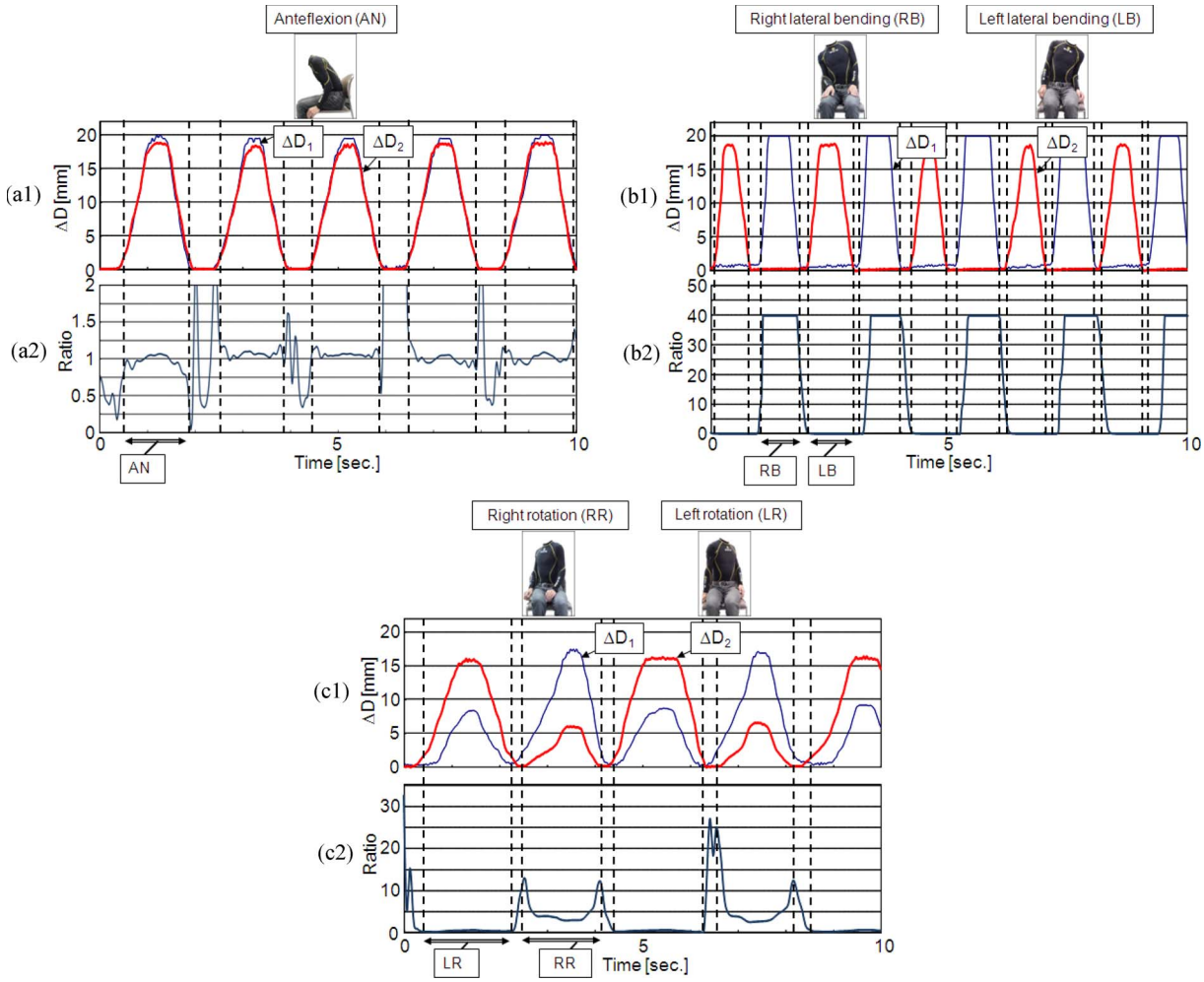

Fig. 12. Experimental results for the repeated trunk motions, showing $\Delta D_{1,2}$ and ratio $\Delta D_1/\Delta D_2$. (a1) and (a2) For anteflexion. (b1) and (b2) For lateral bending. (c1) and (c2) For rotation.

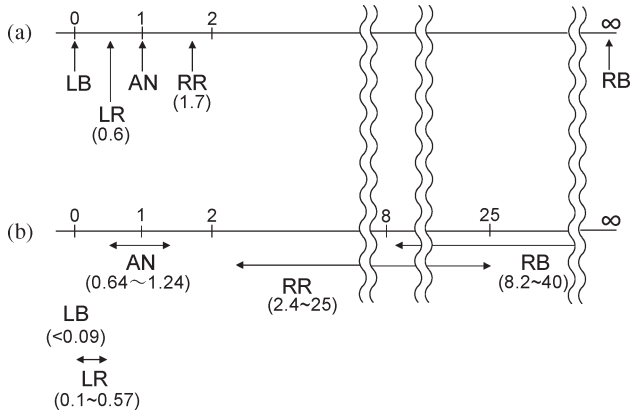

Fig. 13. Ranges of ratio $\Delta D_1/\Delta D_2$ obtained by (a) calculations and (b) experiments.

shown in the upper inset in Fig. 14. After the initial calibration by keeping the posture upright for about 3 s, the process of taking a back swing, which is the combined motion of both left lateral bending and right rotation, was performed from the initial address-posture corresponding to anteflexion. The swing was performed after keeping the same posture with the back swing for about 1 s.

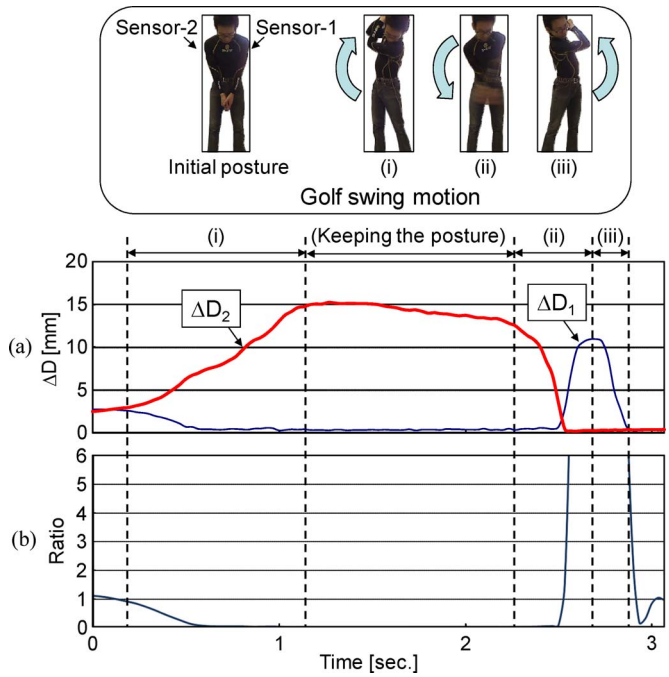

Fig. 14. Real-time response of (a) $\Delta D_{1,2}$ and (b) the ratio $\Delta D_1/\Delta D_2$ for a golf swing motion consisting of (i) taking a backswing, (ii) leading up to the impact, and (iii) following through.

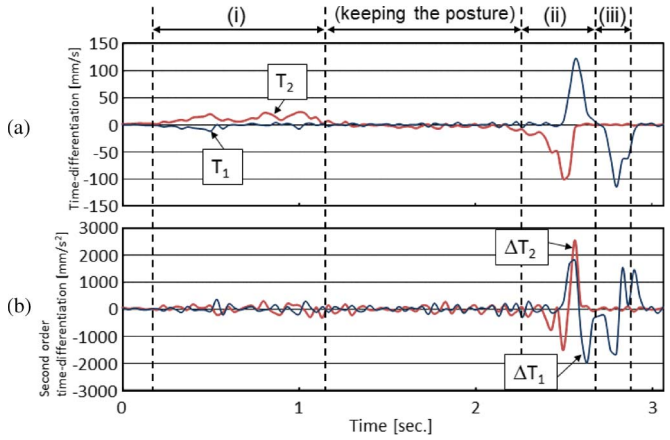

Fig. 15. Time differentiations of ΔD_1 and ΔD_2. (a) The relative velocity and (b) the relative acceleration for the golf swing performed.

Fig. 14(a) shows the real-time responses of two stretch sensors for the swing. The change in ΔD_1 and ΔD_2 indicates that the sensor successfully shows the combined motion of three types of fundamental motions at the trunk in the golf swing process, in accordance with recorded video pictures. Fig. 14(b) shows the ratio $\Delta D_1/\Delta D_2$, in which the ranges are shown as $0 < \Delta D_1/\Delta D_2 < 1$ for (i), 0 for (ii), and $5 < \Delta D_1/\Delta D_2$ for (iii). The change in the ratio as a function of time indicated that the motion of trunk transits from AN to LB for the stage of (i) and from LB to AN for (ii). It is found in Fig. 14(b) that the swing motion could be sufficiently distinguished by evaluating the ratios from the two sensors, even if the motion to be analyzed is formed by a composite of three motions.

Fig. 15 shows the time differentiations for ΔD_1 and ΔD_2, which indicate (a) the relative velocity and (b) the relative acceleration occurring at the sensor modules. In addition, an angular velocity and an acceleration of motion can be also derived from ΔD_1 and ΔD_2 because of ΔD corresponding to angular motion, as mentioned above. These obtained values are useful in knowing how the impulse and the timing in the swing are performed. These results could be applied to other kinds of sports training systems. Although the system used in this experiment needed 1 W/channel for the LED/PD convertor, a wireless system is commercially available by means of a Bluetooth device [22] with a small power consumption of 100 mW per channel.

VII. Conclusion

In this paper, the motion monitor has been described using sportswear in which hetero-core optical fiber sensor modules are sewed so as to be sensitive to stretch on the wear. The accuracy of this technique is closely dependent on what type of cloth and how tight it is, how and where the sensor is sewed or placed on the arm, to what extent the elbow size is, and so on. This technique mainly offers a motion monitor with which people can know the status of their posture, rather than the accurate angle of interest. In other words, the above thing could be a shortcoming of this sensitive sportswear in terms of the expense in achieving higher accuracy. However, a displacement sensor using a hetero-core element, which was previously reported in our paper [20], showed high accuracy with 0.1% for the full scale of 5 mm. This means that an accurate angle gauge can be developed when a hetero-core element is properly mounted in a robust mechanical structure intended only for obtaining accurate angle detection. Depending on the demands of measurement, the integration system of this technique and other inertial sensors could be attractive in accordance with desired applications. The trunk motion could be monitored as well as an elbow joint motion with minimum restriction to the human body. Three types of motion at the trunk have been captured and analyzed by means of the proposed two-plane model for the motions of anteflexion, lateral bending, and rotation. Additionally, the real-time monitoring system has been tested to examine the golf swing motion. In conclusion, it is found that sports motion could be analyzed from view actual points by evaluating the ratios from the two sensor outputs, even if the motion consists of a composite of three motions, with showing the viability to an unconstrained motion capture system intended for an assistance device in sports and rehabilitation fields.

References

[1] S. Williams, R. Schmidt, C. D. Klug, and G. Rau, "An upper body model for the kinematical analysis of the joint chain of the human arm," *J. Biomech.*, vol. 39, no. 13, pp. 2419–2429, Sep. 2006.

[2] I. Boniolo, M. Tanelli, and S. M. Savaresi, "Roll angle estimation in two-wheeled vehicles," *IET Control Theory Appl.*, vol. 3, no. 1, pp. 20–32, Jan. 2009.

[3] G. X. Lee, K. S. Low, and T. Taher, "Unrestrained measurement of arm motion based on a wearable wireless sensor network," *IEEE Trans. Instrum. Meas.*, vol. 59, no. 5, pp. 1309–1317, May 2010.

[4] D. H. Wang and G. Yuan, "A six-degree-of-freedom acceleration sensing method based on six coplanar single-axis accelerometers," *IEEE Trans. Instrum. Meas.*, vol. 60, no. 4, pp. 1433–1442, Apr. 2011.

[5] Z. Q. Zhang and J. K. Wu, "A novel hierarchical information fusion method for three-dimensional upper limb motion estimation," *IEEE Trans. Instrum. Meas.*, vol. 60, no. 11, pp. 3709–3719, Nov. 2011.

[6] R. Takeda, S. Tadano, A. Natorigawa, M. Todoh, and S. Yoshinari, "Gait posture estimation using wearable acceleration and gyro-sensors," *J. Biomech.*, vol. 42, no. 15, pp. 2486–2494, Nov. 2009.

[7] J. Favre, B. M. Jolles, R. Aissaoui, and K. Aminian, "Ambulatory measurement of 3D knee joint angle," *J. Biomech.*, vol. 41, no. 5, pp. 1029–1035, Jan. 2008.

[8] C. K. Lim, Z. Luo, -M. Chen, and S. H. Yeo, "Wearable wireless sensing system for capturing human arm motion," *Sens. Actuators A, Phys.*, vol. 166, no. 1, pp. 125–132, Mar. 2011.

[9] G. A. Borges, A. M. N. Lima, and G. S. Deep, "Characterization of a trajectory recognition optical sensor for an automated guided vehicle," *IEEE Trans. Instrum. Meas.*, vol. 49, no. 4, pp. 813–819, Aug. 2000.

[10] S.-J. Na and S.-W. Park, "Velocity-controlled shape-tracing system using eight optical sensors," *IEEE Trans. Instrum. Meas.*, vol. 37, no. 3, pp. 458–461, Sep. 1988.

[11] M. Norgia, I. Boniolo, M. Tanelli, S. M. Savaresi, and C. Svelto, "Optical sensors for real-time measurement of motorcycle tilt angle," *IEEE Trans. Instrum. Meas.*, vol. 58, no. 5, pp. 1640–1649, May 2009.

[12] C. Berger, "Strain measurement of moving periodic objects with optical sensors," *IEEE Trans. Instrum. Meas.*, vol. 51, no. 4, pp. 616–621, Aug. 2002.

[13] E. P. Scilingo, F. Lorussi, A. Mazzoldi, and D. De Rossi, "Strain-sensing fabrics for wearable kinaesthetic-like systems," *IEEE Sensors J.*, vol. 3, no. 4, pp. 460–467, Aug. 2003.

[14] A. Tognetti, F. Lorussi, R. Bartalesi, S. Quaglini, M. Tesconi, G. Zupone, and D. De Rossi, "Wearable kinesthetic system for capturing and classifying upper limb gesture in post-stroke rehabilitation," *J. NeuroEng. Rehabil.*, vol. 2, no. 8, pp. 1–14, Mar. 2005.

[15] P. T. Gibbs and H. H. Asada, "Wearable conductive fiber sensors for multi-axis human joint angle measurements," *J. NeuroEng. Rehabil.*, vol. 2, no. 7, pp. 1–18, Mar. 2005

[16] A. F. Da Silva, A. F. Goncalves, P. M. Mendes, and J. H. Correia, "FBG sensing glove for monitoring hand posture," *IEEE Sensors J.*, vol. 11, no. 10, pp. 2442–2448, Oct. 2011.

[17] L. Danisch, K. Englehart, and A. Trivett, "Spatially continuous six degree of freedom position and orientation sensor," *Sens. Rev.*, vol. 19, no. 2, pp. 106–112, Feb. 1999.
[18] M. Donno, E. Palange, F. Di. Nicola, G. Bucci, and F. Ciancetta, "A new flexible optical fiber goniometer for dynamic angular measurements: Application to human joint movement monitoring," *IEEE Trans. Instrum. Meas.*, vol. 57, no. 8, pp. 1614–1620, Aug. 2008.
[19] K. Watanabe, K. Tajima, and Y. Kubota, "Macrobending characteristics of a hetero-core splice fiber optic sensor for displacement and liquid detection," *IEICE Trans. Electron.*, vol. E83-C, no. 3, pp. 309–314, Mar. 2000.
[20] H. Sasaki, Y. Kubota, and K. Watanabe, "Sensitivity property of a hetero-core splice fiber optic displacement sensor," in *Proc. SPIE*, 2004, vol. 5579, pp. 136–143.
[21] M. Nishiyama, H. Sasaki, and K. Watanabe, "Performance characteristics of wearable embedded hetero-core fiber sensors for unconstrained motion analyses," *Trans. SICE*, vol. 43, no. 12, pp. 1075–1081, Dec. 2007.
[22] [Online]. Available: http://www.core-system.jp/pdf/i-line%20BOX8B.pdf

Yuya Koyama received the B.E. and M.E. degrees in information systems science from Soka University, Tokyo, Japan, in 2008 and 2010, respectively. He is currently working toward the D.E. degree in hetero-core fiber optic sensor and its application at Soka University.

Michiko Nishiyama received the B.S. degree in physics from Ochanomizu University, Tokyo, Japan, in 2000 and the M.E. and Ph.D. degrees in information systems science from Soka University, Tokyo, in 2005 and 2008, respectively.

From 2000 to 2003, she was with Nikon, designing an optical lens system. From 2008 to 2011, she was an Assistant Professor with Soka University, working on the development of optical fiber sensors. She is currently a Research Associate with the Japan Aerospace Exploration Agency, working on the development of optical fiber sensors for aerospace application.

Kazuhiro Watanabe received the B.E., M.E., and D.E. degrees in electrical engineering from Keio University, Yokohama, Japan, in 1976, 1978, and 1981, respectively.

From April 1981 to March 1991, he was with the Department of Electrical Engineering, National Defense Academy, Yokosuka, Japan, where he was engaged in the development of high-power gas lasers. In April 1991, he joined the Department of Information Systems Science, Soka University, Tokyo, Japan, as an Associate Professor, and in 1996, he became a Professor in the same university. His current research interests include applications of fiber optic sensors and laser machining using femtosecond short pulse lasers.